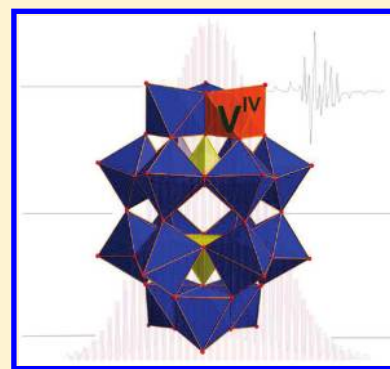


Exploring the Structure and Properties of Transition Metal Templated  $\{VM_{17}(VO_4)_2\}$  Dawson-Like CapsulesHaralampos N. Miras,<sup>\*,†</sup> Daniel Stone,<sup>‡</sup> De-Liang Long,<sup>†</sup> Eric J. L. McInnes,<sup>‡</sup> Paul Kögerler,<sup>§</sup> and Leroy Cronin<sup>\*,†</sup><sup>†</sup>WestCHEM, Department of Chemistry, The University of Glasgow, University Avenue, Glasgow G12 8QQ, Scotland, United Kingdom<sup>‡</sup>The EPSRC UK National Electron Paramagnetic Resonance Service at The University of Manchester, School of Chemistry, Manchester M13 9PL, United Kingdom<sup>§</sup>Institut für Anorganische Chemie, RWTH Aachen University, D-52074, Aachen, Germany and Peter Grünberg Institute—PGI-6, Research Centre Jülich, D-52425 Jülich, Germany

Supporting Information

**ABSTRACT:** Vanadate(V)-templated Dawson-type capsules  $\{V^{IV}M^{VI}_{17}(VO_4)_2\}$  ( $M = Mo, W; 1-2$ ) have been synthesized and investigated by electrochemical methods in aqueous and organic media using spectroscopic techniques, EPR, UV-vis/NIR, IR, and CSI-MS (cryospray ionization mass spec.), and the clusters have been examined in the solid state by magnetic studies. The collision-induced dissociation (CID-MS) studies confirmed the solution structures as well as helped pinpoint the position of the vanadium ion on the  $\{VM_{17}\}$ -type shell, which was corroborated by EPR and theoretical studies.



## INTRODUCTION

Early transition metals (V, Nb, Ta, Mo, W) in their highest oxidation state form discrete polynuclear cluster oxoanions (polyoxometalates, or POMs) which may also incorporate a variety of heteroatoms.<sup>1-3</sup> Owing to their nanoscale structures and properties, POMs are often referred to as soluble metal-oxide fragments and are receiving considerable attention. In this context, POM clusters are unmatched, not only in terms of their structural diversity but also regarding reactivity and electronic properties. For instance, one of the most important properties of POMs is their ability to accept and release specific numbers of electrons reversibly, with negligible structural rearrangement (often referred to as “type I” POMs, according to the classification of Pope).<sup>1,4</sup> In fact, the diverse range of structural and electronic properties associated with POMs means that they have been studied in a range of application areas from catalysis<sup>5-7</sup> to magnetism,<sup>8,9</sup> redox chemistry,<sup>10,11</sup> and materials science.<sup>12-15</sup> In particular, the highly acidic properties of the thermodynamically very stable Keggin-type heteropolyanions (HPAs)<sup>6</sup> such as  $[W_{12}O_{36}(PO_4)]^{3-}$  or the vanadium-substituted polyoxoanions<sup>16</sup> such as  $[H_2V_2Mo_{10}O_{36}(PO_4)]^{3-}$  render such POMs as versatile homogeneous catalysts for catalytic conversion of numerous organic substrates.<sup>17,18</sup> In these systems, the relative acidity and redox properties are critically dependent on the nature and the relative positions of the metal cations in the

POM framework as well as the type of heteroatom template incorporated within the framework.<sup>6,19</sup>

POM clusters also are important for the development of “model” magnetic molecules. This is because the incorporation of exchange-coupled paramagnetic transition-metal ions into the POM frameworks may result in molecules with high spin ground states, pronounced magnetic anisotropies, frustrated ordering, etc.<sup>20</sup> Such materials are ultimately of technical interest in the areas of quantum computing<sup>21a</sup> or molecular electronics.<sup>21b</sup> With this in mind, we recently reported a family of redox-active sulfite-based polyoxomolybdates of the Dawson type  $[Mo_{18}O_{54}(SO_3)_2]^{n-}$ . Here, the integration of pyramidal  $SO_3^{2-}$  anions into the central cavity of such polyoxomolybdates gives rise to unprecedented structural<sup>23,24</sup> and physical<sup>25</sup> features. In an extension of this approach, we recently isolated the first mixed-metal (V/Mo and V/W) vanadate-templated capsules derived from the  $\alpha$ -Dawson structure type, with the composition  $\{VM_{17}(VO_4)_2\}$ .<sup>24</sup> The synthesis employed hydrothermal conditions and bulky (“shrink wrapping”)<sup>26</sup> organic cations, while the *in situ* formation and stability of both polymolybdate and -tungstate capsules can be monitored by cryospray mass spectrometry. The experimental conditions of the reaction solution can be fine-tuned to influence

Received: May 5, 2011

Published: July 27, 2011

the direction of the equilibrium in aqueous media and promote the self-organization of the readily available POM synthons. Herein, we report the physicochemical investigation of the  $\{\text{VM}_{17}(\text{VO}_4)_2\}$  capsules along with detailed CID-MS studies, which allows us to pinpoint the precise location of the framework vanadium  $\text{V}^{\text{IV}}$  metal center within the cluster cage.

## EXPERIMENTAL SECTION

**General Considerations.** All commercially obtained reagents were used without any further purification. Deionized water was used throughout the study.

**Synthesis of  $(\text{Na})_4(\text{NH}_4)_2[\alpha\text{-H}_2\text{VW}_{17}\text{O}_{54}(\text{VO}_4)_2]$  (1).**  $\text{Na}_2\text{WO}_4 \cdot 2\text{H}_2\text{O}$  (1.36 g, 4.1 mmol) and  $\text{NH}_2\text{OH} \cdot \text{HCl}$  (1.3 g, 18.8 mmol) were dissolved in water (10 mL). Upon the addition of  $\text{NH}_2\text{OH} \cdot \text{HCl}$ , precipitation of a white solid occurred almost immediately. The solution was stirred for 2 min followed by the addition of  $\text{NH}_4\text{VO}_3$  (0.2 g, 1.7 mmol). Hydrochloric acid (37%, ~3 mL) was added to the stirred solution, and the pH value of the solution was adjusted to 3.8. The mixture was enclosed in an autoclave, heated up to 160 °C for 3 days, and cooled down. The mixture was filtered and left standing at room temperature in an open Erlenmeyer flask for 5 days, during which time dark purple block crystals suitable for X-ray crystal analysis were collected, washed with a minimum amount of cold ethanol, and dried in the air (yield: 0.99 g, 89%). IR bands (KBr):  $\nu$  3434, 1625 ( $\text{H}_2\text{O}$ ), 957 ( $\text{V}=\text{O}$ ), 915 ( $\text{W}=\text{O}$ ), 891, 856, 760 ( $\text{O}-\text{M}-\text{O}$ )  $\text{cm}^{-1}$ . UV-vis ( $\text{H}_2\text{O}$ ):  $\lambda_{\text{max}}$  ( $\epsilon$ ) 247 (15 300), 312 (11 580), 554 (378) nm ( $\text{dm}^3 \text{mol}^{-1} \text{cm}^{-1}$ ). TGA, percentage weight loss (temperature): 4.67 (160 °C, assigned to  $\text{H}_2\text{O}$ ), 0.73 (208 °C, assigned to  $\text{NH}_3$ ). Elemental analysis (%), calcd. for  $\text{H}_{32}\text{N}_2\text{O}_{74}\text{Na}_4\text{W}_{17}\text{V}_3$ : H, 0.69; N, 0.60; Na, 1.99; V, 3.31; W, 67.70.; Found: H, 0.62; N, 0.71; Na, 2.14; V, 3.38; W, 67.95.

**Synthesis of  $(\text{nBu}_4\text{N})_6[\alpha\text{-H}_2\text{VW}_{17}\text{O}_{54}(\text{VO}_4)_2]$  (2).** The previously reported cation exchange process was followed.<sup>24</sup> The identity and purity of the compound was confirmed by FT-IR spectroscopy.

**Synthesis of  $(\text{TEAH})_6[\alpha\text{-H}_2\text{VMO}_{17}\text{O}_{54}(\text{VO}_4)_2]$  (3).**  $\text{Na}_2\text{MoO}_4 \cdot 2\text{H}_2\text{O}$  (1.3 g, 4.1 mmol) and triethanolamine (TEA; 1.6 g, 8.6 mmol) were dissolved in water (12 mL). Upon the addition of TEA, precipitation of a white solid occurred almost immediately, which redissolved gradually. The solution was stirred for 2 min followed by the addition of  $\text{NH}_4\text{VO}_3$  (0.2 g, 1.7 mmol). Hydrochloric acid (37%, ~3 mL) was added to the stirred orange solution, and the pH value was adjusted to 1.2. The mixture was refluxed for 10 h and cooled down slowly within one day, after which time dark green block crystals suitable for X-ray crystal analysis were collected by filtration, washed with the minimum amount of cold ethanol, and dried in the air (yield: 0.80 g, 91%). IR bands (KBr):  $\nu$  3439, 1621 ( $\text{H}_2\text{O}$ ), 969 ( $\text{V}=\text{O}$ ), 939 ( $\text{Mo}=\text{O}$ ), 897, 861, 758 ( $\text{O}-\text{M}-\text{O}$ )  $\text{cm}^{-1}$ . UV-vis ( $\text{H}_2\text{O}$ ):  $\lambda_{\text{max}}$  ( $\epsilon$ ) 240 (21 100), 309 (16 890), 591 (532) nm ( $\text{dm}^3 \text{mol}^{-1} \text{cm}^{-1}$ ). TGA, percentage weight loss (temperature): 3.81 (170 °C, assigned to  $\text{H}_2\text{O}$ ), 23.56 (up to 800 °C, assigned to  $\text{TEAH}^+$  cations). Elemental analysis (%), calcd. for  $\text{C}_{36}\text{H}_{96}\text{N}_6\text{Mo}_{17}\text{V}_3\text{O}_{80}$ : C, 11.33; H, 2.51; N, 2.20; V, 4.00; Mo, 42.63. Found: C, 11.39; H, 2.65; N, 2.12; V, 4.08; Mo, 42.50.

**Synthesis of  $(\text{nBu}_4\text{N})_6[\alpha\text{-H}_2\text{VMO}_{17}\text{O}_{54}(\text{VO}_4)_2]$  (4).** The previously reported cation exchange process was followed.<sup>24</sup> The identity and purity of the compound was confirmed by FT-IR spectroscopy.

**UV/Vis Spectroscopy.** Deionized water was used as a solvent throughout, which was obtained by passing through a PureLab Option purification set. All solvents were of high-purity grade and were used as purchased without further purification. The UV-vis spectra were recorded on a Perkin-Elmer Lambda 19 spectrophotometer using 1.0 cm optical path quartz cuvettes.

**Flame Atomic Absorption Spectrometry (FAAS).** FAAS was performed at the Environmental Chemistry Section, Department of

Chemistry, University of Glasgow on a Perkin-Elmer 1100B Atomic Absorption Spectrophotometer.

**Microanalysis.** Carbon, nitrogen, and hydrogen contents were determined by the microanalysis services within the Department of Chemistry, University of Glasgow using an EA 1110 CHNS, CE-440 Elemental Analyzer.

**Fourier-Transform Infrared (FT-IR) Spectroscopy.** Unless stated otherwise, the materials were prepared as KBr pellets, and FT-IR spectra were collected in transmission mode using a JASCO FT-IR 4100 spectrometer.

**Thermogravimetric Analysis (TGA).** Thermogravimetric analysis was performed on a TA Instruments Q 500 Thermogravimetric Analyzer under a nitrogen flow at a typical heating rate of 5 °C  $\text{min}^{-1}$ .

**Electrochemical Experiments.** The solutions were deaerated thoroughly for at least 15 min with pure argon and kept under a positive Ar pressure during the experiments. The source, mounting, and polishing of the glassy carbon (GC) electrodes have been described previously.<sup>11b</sup> The glassy carbon samples had a diameter of 3 mm. A VoltaLab 400 potentiostat was used. Potentials are quoted against Ag/AgCl. The counter electrode was platinum gauze of large surface area. All experiments were performed at room temperature ( $19 \pm 1$  °C).

**CID-MS Experimental and Analyses.** All MS data were collected using a Q-trap, time-of-flight MS (MicrOTOF-QMS) instrument supplied by Bruker Daltonics Ltd. The detector was a time-of-flight, microchannel plate detector, and all data were processed using the Bruker Daltonics Data Analysis 3.4 software, while simulated isotope patterns were investigated using Bruker Isotope Pattern software and Molecular Weight Calculator 6.45. The following parameters were consistent for all CID-MS scans given below. The calibration solution used was Agilent ES tuning mix solution, Recorder No. G2421A, enabling calibration between approximately 100  $m/z$  and 3000  $m/z$ . This solution was diluted 60:1 with MeCN. Samples were introduced into the MS via direct injection at 180  $\mu\text{L}/\text{h}$ . The ion polarity for all MS scans recorded was negative, at 25 °C, with the voltage of the capillary tip set at 4000 V, the end plate offset at -500 V, funnel 1 RF at 300Vpp, and funnel 2 RF at 400Vpp. The collision energy has been increased gradually from an initial value of 5 eV up to the maximum—for the tungsten analogue—of 25 eV.

**X-Ray Crystallography.** Diffraction data sufficient for unit cell determination for compound 1 and 3 were determined on an Oxford Diffraction Gemini Ultra with a CrysAlis CCD detector [Mo K $\alpha$  radiation ( $\lambda = 0.71073$  Å)].

**Magnetic Measurements.** Temperature- and field-dependent magnetic susceptibility data ( $T = 2.0$ –290 K,  $H = 0.1$ –5.0 T) for 1 and 3 were recorded using a Quantum Design MPMS-5 SQUID magnetometer. The data were corrected for the contribution of the cylindrical PTFE sample holder and for the diamagnetism and temperature-independent paramagnetism (TIP) of the samples estimated from Pascal constants and measurements on diamagnetic Mo- and W-Dawson species.

**EPR Measurements.** EPR spectra of polycrystalline samples of 2 and 4 were recorded at X- and W-band (ca. 9 and 94 GHz, respectively), between 100 and 300 K, on Bruker EMX and EleXsys spectrometers. Frozen solutions (MeCN) were recorded at X-band and 100 K.

**Density Functional Theory Studies.** Density functional theory calculations were performed using Turbomole 5.9.1 and Jaguar 7.0 on cluster ions in a surrounding field of +1 point charges. TZVP basis sets and B3-LYP hybrid functionals (for final single-point calculations) were used. The model structures were derived from crystallographic sets and were relaxed freely (employing B-P functionals), whereby a doming shift of the V positions out of the  $\mu\text{-O}_4$  plane toward the outer oxo position was observed as expected for a vanadyl group.

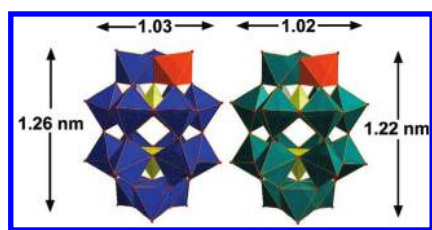


**Figure 1.** Representations of the iso-structural frameworks found in the structures of compounds 1–4 with the framework V shown in the cap region, as suggested by this work (the compounds are formally shown without counterions or solvent), with the general formula  $[\text{H}_2\text{VM}_{17}\text{O}_{54}(\text{VO}_4)_2]^{6-}$  ( $\text{M} = \text{W}$  or  $\text{Mo}$ ). Color scheme: W, blue polyhedra; Mo, green polyhedra; O, red spheres;  $\text{V}^{\text{V}}$ , yellow polyhedra;  $\text{V}^{\text{IV}}$ , orange polyhedra.

## RESULTS AND DISCUSSION

The synthesis of **1** and **3** presented here minimizes the side products with the aim of maximizing the yield,<sup>24</sup> compared to the previous synthesis. This was achieved by adjusting the pH to an optimum value (3.8) in the region of pH values where **1** can be isolated. Then, the mixture was cooled to room temperature, and any powdery insoluble impurity was removed by filtration. The clear dark purple filtrate was kept in a flask at room temperature for 5 days. After this period of time, crystals that were formed were removed by filtration every two days up to the point that the filtrate turned green and no more crystalline material was produced. In the case of compound **3**, the pH was adjusted exactly to the value of 1.2 along with an increase in the amount of TEA, which also improved the rate of cluster formation (10 h refluxing instead of  $\sim 24$  h). It is necessary to avoid the addition of excessive amounts of TEA in order to avoid cocrystallization and consequently contamination of the desirable green crystalline product. The products have been characterized by analytical and spectroscopic methods (see Experimental Section) as well as by crystallographic investigations. The  $\{\text{M}_{17}\text{V}_3\}$  capsule consists of an 18-metal-center shell  $[\text{M}: \text{W}$  (**1**),  $\text{Mo}$  (**2**)] where two vanadium  $\text{V}^{\text{V}}$  centers occupy the two vacant interior positions, while an additional  $\text{V}^{\text{IV}}$  center resides on the shell (Figure 1). The dimensions observed for the two capsules are  $1.26 \times 1.03$  and  $1.22 \times 1.02$  nm for the  $\{\text{W}_{17}\text{V}_3\}$  and  $\{\text{Mo}_{17}\text{V}_3\}$  clusters, respectively. Interestingly, the CSI-MS studies have proven to be a powerful analytical approach to investigating POM-based systems.<sup>25e</sup> Also, using collision-induced dissociation (CID) experiments, we were able to explore the routes of cluster decomposition by a gradual increase of the collision energy inducing fragmentation of the parent architecture, and this allowed us to determine the exact location (cap or belt site) of the reduced vanadium center on the shell of the Dawson capsule. Furthermore, the above data were found to be in excellent agreement with the EPR and theoretical calculations studies (see below).

**Insights Gained from CID-MS Studies.** Despite the increasing interest in POM-based materials, an accurate determination of the formula, structure, and understanding of the assembly process still represents a great challenge, which is crucial for further synthetic development and exploitation. However, the use of electrospray mass spectrometry (ESI-MS) to investigate POM systems as a complementary technique to X-ray crystallography and NMR studies has increased steadily over the past decade.<sup>25–27</sup> Recently, in some of our previous work, we demonstrated that electrospray (ESI-) and cryospray mass

**Table 1.** Detected Species during the CID Experiments for Compound **2**

$m/z$		peak assignment
experimental	simulated	
560.80	560.86	$[\text{Na}_2\text{W}_2\text{O}_9\text{H}_3]^-$
1000.70	1000.77	$[\text{Na}_9\text{W}_3\text{O}_{14}(\text{H}_2\text{O})]^-$
1186.01	1186.02	$[\text{TBAW}_4\text{O}_{13}]^-$
1258.59	1258.60	$[\text{W}_5\text{O}_{14}(\text{VO}_4)]^-$
1413.00	1412.94	$[\text{TBA}_3\text{W}_{14}\text{O}_{44}(\text{VO}_4)_2\text{H}_4]^{3-}$
1457.10	1456.94	$[\text{TBA}_3\text{W}_{15}\text{O}_{48}(\text{VO}_4)\text{H}_3]^{3-}$
1490.66	1490.61	$[\text{TBA}_3\text{W}_9\text{O}_{30}(\text{VO}_4)\text{H}_4]^{2-}$
1517.63	1517.56	$[\text{TBA}_3\text{VW}_{15}\text{O}_{49}(\text{VO}_4)\text{H}_3]^{3-}$
1543.05	1542.90	$[\text{TBA}_3\text{VW}_{15}\text{O}_{52}\text{Na}(\text{VO}_4)_2\text{H}_8]^{3-}$
1579.47	1579.57	$[\text{TBA}_3\text{W}_{16}\text{O}_{52}(\text{VO}_4)_2\text{H}_8]^{3-}$
1604.07	1603.99	$[\text{TBA}_4\text{V}^{\text{V}}\text{W}_{15}\text{O}_{50}(\text{VO}_4)_2\text{H}_4]^{3-}$
1666.17	1666.18	$[\text{TBA}_3\text{VW}_{17}\text{O}_{54}(\text{VO}_4)_2\text{H}]^{3-}$

spectrometry (CSI-MS) can be a powerful tool in studying complex chemical systems in solution such as POMs and supramolecular coordination clusters, allowing the elucidation of the formula and providing insight into the “building-blocks” present in solution.<sup>25</sup> Since the CSI-MS studies can provide fragmentation data, it may be possible to correlate the observed data with possible mechanisms of decomposition of the compounds. Further, the fragmentation data may also give some insights regarding the assembly of the clusters. In this respect, it is vital to point out that fragmentation studies are intrinsically limited with regard to mechanistic information for self-assembly, but at the same time such data may be useful to compare and contrast with direct observations of the solutions of the materials undergoing the self-assembly process. In the context of this work, the CID studies should allow us to pinpoint the location of the framework vanadium ion as long as scrambling is not observed under the conditions of the experiment.

In our previous work, utilization of CSI-MS studies allowed us to observe that the clusters retain their structural integrity in  $\text{CH}_3\text{CN}$  solution while helping us define unambiguously the extent of protonation. On the basis of our previous observations, we conducted CID experiments for the organic soluble version of the  $\{\text{VM}_{17}(\text{VO}_4)_2\}$  capsules (**2** and **4**) in  $\text{CH}_3\text{CN}$  in an effort to identify the stable “intermediate” species in solution, which could help define the exact location of the reduced vanadium(IV) center on the shell of the cage. The peaks observed during the course of the CID experiments for compound **2** (Table 1 and Figure 2) are associated with the species  $[\text{Na}_2\text{W}_2\text{O}_9\text{H}_3]^-$ ,  $[\text{Na}_9\text{W}_3\text{O}_{14}(\text{H}_2\text{O})]^-$ ,  $[\text{TBAW}_4\text{O}_{13}]^-$ ,  $[\text{W}_5\text{O}_{14}(\text{VO}_4)]^-$ ,  $[\text{TBA}_3\text{W}_{14}\text{O}_{44}(\text{VO}_4)_2\text{H}_4]^{3-}$ ,  $[\text{TBA}_3\text{W}_{15}\text{O}_{48}(\text{VO}_4)\text{H}_3]^{3-}$ ,  $[\text{TBA}_3\text{W}_9\text{O}_{30}(\text{VO}_4)\text{H}_4]^{2-}$ ,  $[\text{TBA}_3\text{V}^{\text{V}}\text{W}_{15}\text{O}_{49}(\text{VO}_4)\text{H}_3]^{3-}$ ,  $[\text{TBA}_3\text{W}_{15}\text{O}_{52}(\text{VO}_4)_2\text{NaH}_8]^{3-}$ ,  $[\text{TBA}_3\text{W}_{16}\text{O}_{52}(\text{VO}_4)_2\text{H}_8]^{3-}$ ,  $[\text{TBA}_4\text{V}^{\text{V}}\text{W}_{15}\text{O}_{50}(\text{VO}_4)_2\text{H}_4]^{3-}$ , and  $[\text{TBA}_3\text{VW}_{17}\text{O}_{54}(\text{VO}_4)_2\text{H}]^{3-}$ , while the respective ones for compound **4** can be assigned to the species  $[\text{TBA}_2\text{Mo}^{\text{V}}_2\text{Mo}^{\text{VI}}_3\text{O}_{15}(\text{VO}_4)\text{H}_2]^-$ ,  $[\text{TBA}_2\text{V}^{\text{IV}}\text{Mo}^{\text{VI}}_5\text{O}_{17}(\text{VO}_4)]^-$ ,  $[\text{TBAV}\text{Mo}^{\text{V}}_2\text{Mo}^{\text{VI}}_6\text{O}_{25}(\text{VO}_4)\text{H}]^-$ ,  $[\text{TBA}\text{Mo}^{\text{V}}_6\text{Mo}^{\text{VI}}_3\text{O}_{25}(\text{VO}_4)\text{H}_3]^-$ ,  $[\text{TBAV}^{\text{IV}}\text{Mo}^{\text{V}}_7\text{Mo}^{\text{VI}}_2\text{O}_{25}(\text{VO}_4)]^-$ ,  $[\text{TBA}_4\text{V}^{\text{IV}}\text{Mo}^{\text{VI}}_4\text{O}_{14}(\text{VO}_4)\text{H}_2]^-$ ,  $[\text{TBA}_4\text{V}^{\text{V}}\text{Mo}_{17}\text{O}_{54}(\text{VO}_4)_2\text{H}]^{2-}$ , and  $[\text{TBA}_2\text{Mo}^{\text{VI}}_9\text{O}_{27}(\text{VO}_4)]^-$ , respectively (Table 2, Figure 3).

A first important observation is that the tungsten-based synthons proved to be more stable under the experimental conditions. Consequently, it is possible to imagine possible

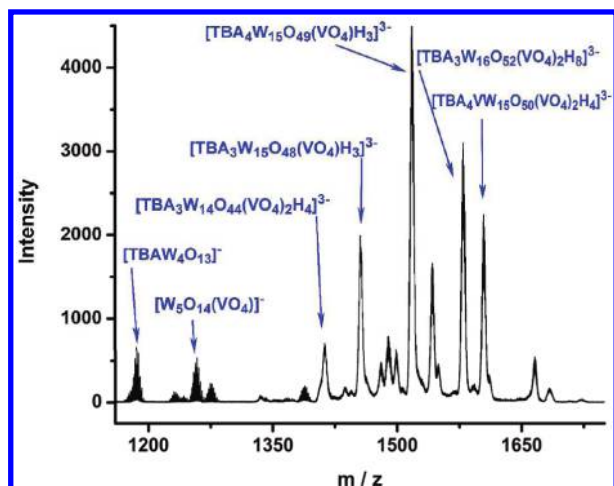


**Figure 2.** Mass spectral data of 2 recorded using collision-induced dissociation (CID) of the isolated  $[\text{TBA}_3\text{VW}_{17}\text{O}_{54}(\text{VO}_4)_2\text{H}_2]^{3-}$  peak at 1666.1  $m/z$  (see Supporting Information for more details).

**Table 2.** Detected Species in the CID Experiments for Compound 4

$m/z$		peak assignment
experimental	simulated	
1320.95	1320.96	$[\text{TBA}_2\text{Mo}_2\text{Mo}_3\text{O}_{15}(\text{VO}_4)\text{H}_2]^-$
1401.88	1401.88	$[\text{TBA}_2\text{V}^{\text{IV}}\text{Mo}_5\text{O}_{17}(\text{VO}_4)]^-$
1593.28	1593.27	$[\text{TBAVMo}_2\text{Mo}_6\text{O}_{25}(\text{VO}_4)\text{H}]^-$
1624.21	1624.25	$[\text{TBA}\text{Mo}_6\text{Mo}_6\text{O}_{25}(\text{VO}_4)\text{H}_3]^-$
1672.21	1672.17	$[\text{TBAV}^{\text{IV}}\text{Mo}_7\text{Mo}_6\text{O}_{25}(\text{VO}_4)]^-$
1695.66	1695.63	$[\text{TBA}_4\text{Mo}_4\text{O}_{14}(\text{VO}_4)\text{H}_2]^-$
1874.04	1874.03	$[\text{TBA}_4\text{V}^{\text{IV}}\text{Mo}_{17}\text{O}_{54}(\text{VO}_4)_2\text{H}_2]^{2-}$
1977.65	1977.56	$[\text{TBA}_2\text{Mo}_9\text{O}_{27}(\text{VO}_4)]^-$

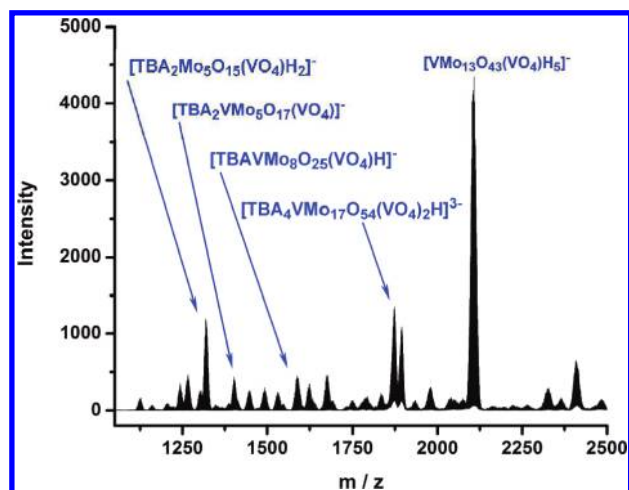


**Figure 3.** Mass spectral data of 4 recorded using collision-induced dissociation (CID) of the isolated  $[\text{TBA}_4\text{VMo}_{17}\text{O}_{54}(\text{VO}_4)_2\text{H}_2]^{3-}$  peak at 1874.0  $m/z$  (see Supporting Information for more details).

building blocks that could underpin the self-assembly of the cluster involving the gradual growth from a  $\{\text{W}_4\}$  to V-templated  $\{\text{W}_9\}$  building block and finally to the  $\{\text{VW}_{17}(\text{VO}_4)_2\}$  capsule

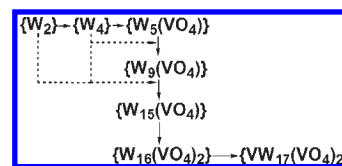


**Figure 4.** Proposed condensation process and stable synthons for the tungsten/vanadium system based on the mass spectral data recorded using collision-induced dissociation (CID).

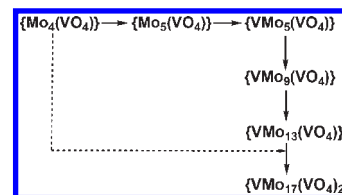


**Figure 5.** Proposed condensation process and stable synthons for the molybdenum/vanadium system based on the mass spectral data recorded using collision-induced dissociation (CID).

via the formation of higher nuclearity “lacunary” species  $[\{\text{W}_{15}\}]$  and  $\{\text{W}_{16}\}$  (Figure 4). Of course, it is not possible to use CID studies to elucidate mechanistic pathways directly since the process involves the decomposition of the cluster in  $\text{CH}_3\text{CN}$ , yet the information yielded can be useful to at least postulate some ideas that could then be used to form testable hypotheses.

In the case of the Mo-based capsules, the system showed a relative inability to retain the integrity of smaller fragments  $[\{\text{Mo}_1\} - \{\text{Mo}_3\}]$  at increased values of collision energy. Instead, the suggested mechanism is based on the formation of higher nuclearity  $\text{VO}_4$ -templated fragments, which leads to the construction of the final product through four stages (Figure 5). This can be explained if we take into consideration the relative lability of molybdenum in comparison to tungsten.

These observations give us valuable information regarding the potential mechanism of formation of the two chemical systems as well as the stability of the synthons that exist in solution. It would appear that, in the Mo-based system, it is necessary to incorporate the  $\{\text{VO}_4\}$  template at the very beginning of the assembly process in order to form the building blocks (e.g.,  $[\text{TBAVMo}_2\text{Mo}_6\text{O}_{25}(\text{VO}_4)\text{H}]^-$  and  $[\text{TBA}_2\text{Mo}_2\text{Mo}_3\text{O}_{15}(\text{VO}_4)\text{H}_2]^-$ ) which undergo further aggregation to form the final product through a condensation process. In the tungsten-based system, the small fragments are much more stable/less labile, while it would appear that it is not necessary to incorporate the template from the very start of the aggregation process.

In both cases, the growth process leads to the formation of the templated half-Dawson lacunary species,  $\{\text{W}_9(\text{VO}_4)\}$  and  $\{\text{V}^{\text{IV}}\text{Mo}_9(\text{VO}_4)\}$ , respectively. Even though these have not been reported in the literature previously, this study suggests that the vanadium templated lacunary species could be stable (this is also based on other reported  $\text{XM}_9$  examples, where  $\text{X} = \text{Ge}, \text{P}, \text{Si}$ , etc.)<sup>28</sup> and could potentially be isolated in the solid state and used as new types of building units.

An important outcome from the above set of data is that it may be postulated that, during the molecular growth process of the W-based capsule, the additional reduced vanadium  $\text{V}^{\text{IV}}$  atom is not incorporated before the formation of the  $\{\text{W}_{16}(\text{VO}_4)_2\}$  lacunary species, which clearly indicates that the metallic center is localized on the cap of the Dawson capsule, in excellent

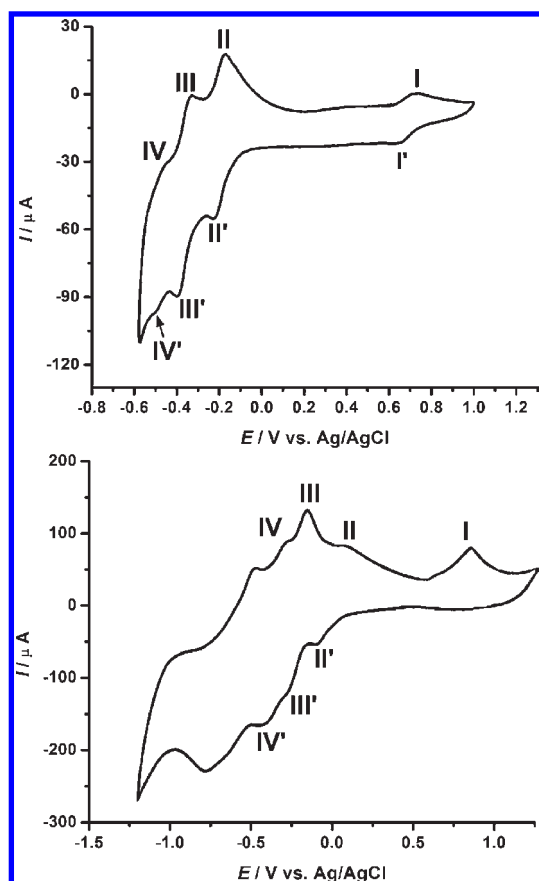


**Figure 6.** Representation of the cyclic voltammograms of  $4 \times 10^{-5}$  M **1** (top) and **3** (bottom) in a pH = 3 medium ( $0.5$  M  $\text{Na}_2\text{SO}_4/\text{H}^+$ ). The working electrode was glassy carbon, and the reference electrode was Ag/AgCl. The scan rate was  $100$   $\text{mVs}^{-1}$ . For further details, see text.

agreement with the theoretical and EPR spectroscopic studies (see below). In the case of the Mo-based capsule, however, the data indicate that there is no preferential framework position for the additional vanadium metal center, and it can either occupy a “cap” or “belt” position. The main reason for this observation is the relative lability of molybdenum and consequently the equilibrium which is established between the free hydrated molybdenum centers with the formed Mo-based intermediate species (Table 2). This indicates that the  $\text{V}^{\text{IV}}$  metal center is delocalized over 18 positions on the capsule’s shell. Again, this is supported by the EPR spectroscopy (see below).

**Electrochemistry.** *Stability Studies.* UV-vis spectroscopy and cyclic voltammetry (CV) were used to assess the stability of the title polyanions by redissolving **1** and **3** in several aqueous media typically used as supporting electrolytes in electrochemical studies of POMs. Both techniques demonstrate that compounds **1** and **3** are stable up to a pH value of 4. In this pH domain, their electronic spectra are characterized by absorption peaks in the visible region located roughly at 310 and 590 nm assigned to IVCT transitions. The locations of these peaks depend on the pH value. During the monitoring process, the UV-vis spectra did not change over a period of 24 h. Voltammograms of  $(\text{TEAH})_6[\text{VMo}_{17}\text{O}_{54}(\text{VO}_4)_2]$  dissolved in aqueous electrolyte media with  $\text{pH} > 4$  showed obvious instability, as faradaic currents decrease relatively quickly with time. Thus, our initial voltammetric studies emphasize  $\text{pH} \leq 4$  conditions.

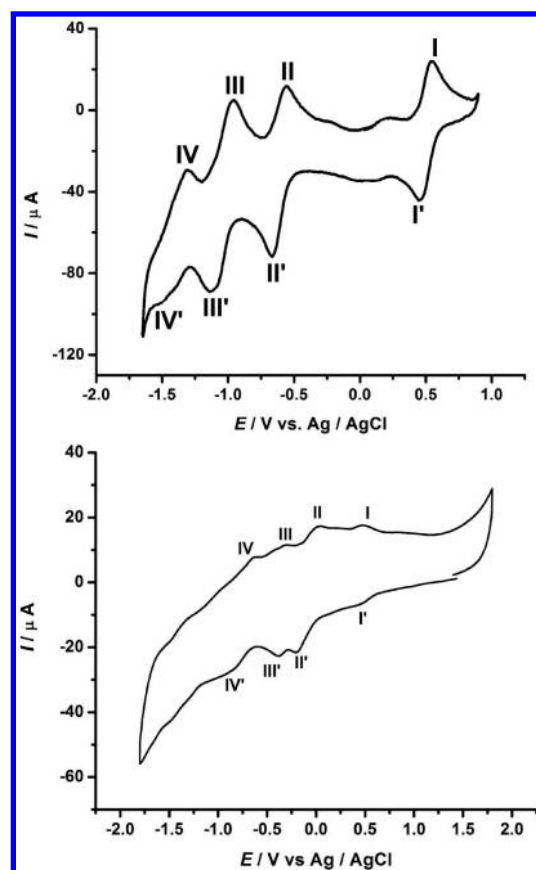


**Figure 7.** Representation of the cyclic voltammograms of  $4 \times 10^{-5}$  M **2** (top) and  $4 \times 10^{-5}$  M **4** (bottom) in dry  $\text{CH}_3\text{CN}$  ( $0.1$  M TBAPF<sub>6</sub>). The working electrode was glassy carbon, and the reference electrode was Ag/AgCl. The scan rate was  $100$   $\text{mVs}^{-1}$ . For further details, see text.

*Voltammetric Studies.* Figure 6 shows the voltammograms of **1** and **3** in an unbuffered ( $\text{pH} = 3$ ) aqueous medium. In the positive region of potentials for compound **1**, we observed an oxidation peak located at  $E_{\text{av}} = 0.690$  V versus Ag/AgCl, while the  $\Delta E_p$  value of  $0.085$  V for the oxidation process of interest suggests a quasi-reversible one-electron process (the theoretical value of  $\Delta E_p$  for a reversible electron transfer is about  $0.059$  V) which does not exist in the pattern of the  $\{\text{X}_2\text{W}_{18}\}$  species.

This wave is assigned to the reversible oxidation of the  $\text{V}^{\text{IV}}$  center. Controlled potential coulometry with the potential set at  $0.700$  V versus Ag/AgCl indicates the consumption of  $1 \pm 0.2$  electron per molecule. Similar behavior was observed in the case of the  $\{\text{V}^{\text{IV}}\text{Mo}_{17}(\text{VO}_4)_2\}$  **2**, where in this case the oxidation of the V center took place at  $+0.610$  V and has been confirmed as a one-electron process as well. Toward the negative region of potentials, three and four quasi-reversible redox couples were observed for the  $\{\text{V}^{\text{IV}}\text{W}_{17}(\text{VO}_4)_2\}$  and  $\{\text{V}^{\text{IV}}\text{Mo}_{17}(\text{VO}_4)_2\}$  capsules, located at  $-0.200$ ,  $-0.363$ , and  $-0.480$  and  $+0.003$ ,  $-0.213$ ,  $-0.349$ , and  $-0.565$  V for compounds **1** and **2**, respectively.

The electrochemical behavior of the same materials was studied in organic solvent as well. Figure 7 shows the voltammograms of **2** and **4** in acetonitrile. In the positive region of potentials for both compounds, we observed an oxidation peak located at  $E_{\text{av}} = 0.496$  V and  $E_{\text{av}} = 0.477$  V versus Ag/AgCl, respectively. The observed reversible couples in the negative region of potentials are assigned to the reversible W- and quasi-reversible overlapping Mo-centered

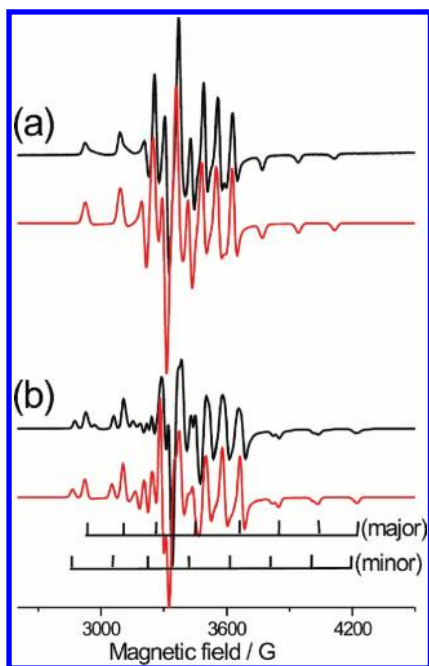


**Figure 8.** X-band EPR spectra of polycrystalline samples of **2** (top) and **4** (bottom) at room temperature: experimental (black) and simulations with the parameters in the text (red). The  $^{51}\text{V}$  hyperfine octets to  $g_3$  for the two distinct structural sites in **4** are indicated.

reduction processes, which are located at  $-0.615$ ,  $-1.065$ , and  $-1.408$  and  $-0.090$ ,  $-0.359$ , and  $-0.741$  V, respectively.

**Magnetic Measurements.** Temperature-dependent magnetic susceptibility studies of **1–4** at 0.1 T show  $\chi_{\text{mol}}T$  values of  $0.36\text{--}0.37$   $\text{cm}^3$  K  $\text{mol}^{-1}$  that remain virtually constant, within the experimental error limit of  $\pm 0.02$   $\text{cm}^3$  K  $\text{mol}^{-1}$ , over the entire experimental temperature range (2.0–290 K). This confirms the presence of a single  $\text{VO}^{2+}$  vanadyl constituent in the  $\text{M}_{18}$  shell structure of each cluster. The corresponding  $S = 1/2$  ground state also results from field-dependent low-temperature magnetization measurements (2.0 K, 0.1–5.0 T), where the onset of magnetic saturation is fully reproduced by  $S = 1/2$  Brillouin functions, yielding  $g_{\text{iso}} = 1.98\text{--}1.99$ . Note that the temperature-independent  $\chi_{\text{mol}}T$  values also rule out a scenario in which the 3d electron is localized on one of the  $\text{VO}_4$  templates ( $^2\text{E}$  ground term), as orbital contributions would cause a temperature dependence of  $\chi_{\text{mol}}T$ .

**EPR Spectroscopy.** In order to probe the locations of the paramagnetic dopant  $\text{V}^{\text{IV}}$  ions ( $d^1$ ,  $s = 1/2$ ), samples of **2** and **4** were studied by EPR. Well-resolved spectra with  $^{51}\text{V}$  hyperfine interactions ( $I = 7/2$ ) are observed from both frozen solution (MeCN) and polycrystalline samples (Figure 8 and Figure S1, Supporting Information). The resolution in the latter shows that the  $\text{V}^{\text{IV}}$  ions are magnetically dilute, and the lack of any structure consistent with  $\text{V}^{\text{IV}} \cdots \text{V}^{\text{IV}}$  interactions is further evidence of the formation of discrete molecules of formula  $\{\text{V}^{\text{IV}}\text{M}_{17}(\text{V}^{\text{V}}\text{O}_4)_2\}$  rather than solid solution distributions. This is also true in solution because the frozen solution and polycrystalline spectra are essentially identical. The spectra of the  $\{\text{V}^{\text{IV}}\text{W}_{17}(\text{V}^{\text{V}}\text{O}_4)_2\}$  species **2** are of a single  $\text{V}^{\text{IV}}$  site (even with the enhanced  $g$ -resolution at the W-band) and can be simulated as such with  $g_1 = 1.972$ ,  $g_2 = 1.977$ ,  $g_3 = 1.923$ ,  $A_1 = A_2 = 60$ , and  $A_3 = 120$  G, where  $g_i$  and  $A_i$  are the electronic  $g$  value and  $^{51}\text{V}$  hyperfine coupling constants, respectively [Figure 8 (top) and Figure S3.1 (top),

Supporting Information]. In contrast, spectra of the  $\{\text{V}^{\text{IV}}\text{Mo}_{17}(\text{V}^{\text{V}}\text{O}_4)_2\}$  species **4** clearly show two distinct, but isolated, species. This is most obviously apparent in the hyperfine structure to the lowest  $g$  value(s) ( $g_3$ ) where two distinct but slightly offset octet patterns are observed [Figure 8 (bottom) and Figure S1 (bottom)]. Simulation requires two independent species, giving  $g_1 = 1.958$ ,  $g_2 = 1.962$ ,  $g_3 = 1.893$ ,  $A_1 = A_2 = 64$ , and  $A_3 = 186$  G for site a and  $g_1 = 1.968$ ,  $g_2 = 1.973$ ,  $g_3 = 1.913$ ,  $A_1 = A_2 = 70$ , and  $A_3 = 192$  G for site b. Matching to the experimental data gives a relative site a/b weighting of 2:1 [Figure 8 (bottom) and Figure S3.1 (bottom)]. Hence, these data are consistent with the mass spectrometry evidence above: the  $\text{V}^{\text{IV}}$  ion in  $\{\text{V}^{\text{IV}}\text{W}_{17}(\text{V}^{\text{V}}\text{O}_4)_2\}$  occupies only one unique site, in one of the six cap sites of the Dawson capsule. In contrast, the  $\text{V}^{\text{IV}}$  ion in  $\{\text{V}^{\text{IV}}\text{Mo}_{17}(\text{V}^{\text{V}}\text{O}_4)_2\}$  occupies one of two unique sites, either in one of the 12 belt sites or in one of the six cap sites. This gives the experimentally observed 2:1 ratio from EPR.

The spectral parameters, with ( $g_c >$ )  $g_1 \approx g_2 > g_3$  and  $|A_1| \approx |A_2| < |A_3|$ , are characteristic of  $\{\text{V}^{\text{IV}}\text{O}\}^{2+}$  vanadyl species; the “unique” axis is associated with the  $\text{V}=\text{O}$  direction (defining the local  $z$  axis) with the unpaired electron in the  $d_{x^2-y^2}$  orbital by simple crystal-field arguments. The differences in parameters between the cap and belt sites for **4** are small, consistent with the similar metric parameters for these sites (e.g.,  $<0.02$  Å differences between equivalent bond lengths).

The parameters for the tungsten compound **2** are very different from those of **4**. The much smaller  $^{51}\text{V}$  hyperfine coupling constants imply greater delocalization of the unpaired electron density. Simple calculations based on the EPR parameters give vanadium  $3d_{x^2-y^2}$  spin densities of 75% for **4** and 34% for **2**. This is presumably due to the greater spatial overlap with valence orbitals from the neighboring metal ions for W (5d) *cf.* Mo (4d).

**DFT Studies.** Open-shell DFT calculations<sup>24</sup> conducted on the  $\{\text{H}_2\text{M}_{17}\text{V}_3\}$  cluster anion (**1a**, **3a**) structures derived from anions of compounds **1** and **3**, in which a single metal position of the  $\{\text{M}_{18}\text{O}_{54}\}$  shell was defined as vanadium, helped us postulate the position of the  $\text{V}^{\text{IV}}$  ion: The total energy favors the isomer with V localized in the two outer  $\text{M}_3$  cap groups over the other possible isomer with V as part of the two central  $\text{M}_6$  belt groups for both the molybdate ( $\Delta E = 12.3$  kJ/mol) and the tungstate ( $\Delta E = 10.7$  kJ/mol) anion; this difference is likely due to the absence of suitable ligand groups positioned *trans* to the vanadyl groups in the belt-substituted isomer. The theoretical calculations proved to be in good agreement with our experimental findings derived from the CID studies. In the case of  $\{\text{H}_2\text{W}_{17}\text{V}_3\}$  **1**, the  $\text{V}^{\text{IV}}$  ion is localized entirely on the  $\text{M}_3$  cap sites of the Dawson capsule. In the case of  $\{\text{H}_2\text{Mo}_{17}\text{V}_3\}$  **3**, the experiment showed that the vanadium metal center can occupy either the  $\text{M}_3$  cap or the less energetically favorable  $\text{M}_6$  belt position. This observation can be explained if we take into account molybdenum’s higher lability under the specific experimental conditions, which allows the occupation of both positions. Furthermore, analysis of the single-occupied, highest molecular orbital shows that the single unpaired electron is localized virtually only on the cluster shell vanadyl group and not on the central  $\text{VO}_4$  templates, so that we can formally assign the central V positions as  $\text{V}^{\text{V}}$  (in agreement with BVS calculations). However, the lowest unoccupied MOs see varying contributions from Mo-(4d) and W(5d) components that reflect the color differences of compounds **1** and **3** (predominantly due to IVCT transitions).

## CONCLUSIONS

In our recent work, we have shown that the self-assembly of POM clusters can be controlled by the cation type, which helped us produce V-templated Dawson-like clusters yielding  $[\alpha\text{-H}_2\text{VW}_{17}\text{O}_{54}(\text{VO}_4)_2]^{6-}$  (1) and  $[\alpha\text{-H}_2\text{VMo}_{17}\text{O}_{54}(\text{VO}_4)_2]^{6-}$  (3). In this work, the above compounds were studied extensively in solution by cryospray mass spectrometry, and a possible location of the  $\text{V}^{\text{IV}}$  ion on the Dawson-like cluster shell was pinpointed. In addition, some possible mechanisms were proposed within the limitations of the technique. These studies imply that the W-based system evolves via the formation of lower nuclearity stable species such as  $\{\text{W}_2\}$ ,  $\{\text{W}_4\}$ , and  $\{\text{W}_5\}$  before the introduction of the  $\{\text{VO}_4\}$  template anion. On the other hand, in the Mo-based system, it is necessary to incorporate the template from the very start of the assembly process in order to form the lower nuclearity synthons which eventually evolve to the final product,  $\{\text{V}^{\text{IV}}\text{Mo}_{17}(\text{V}^{\text{VO}_4})_2\}$ . Another interesting outcome from the CID studies is the fact that we were able to determine the exact location of the  $\text{V}^{\text{IV}}$  on the shell of the Dawson structure. In the case of  $\{\text{V}^{\text{IV}}\text{W}_{17}(\text{V}^{\text{VO}_4})_2\}$ , the vanadium(IV) metal center appears not to be introduced into the framework before the formation of the higher nuclearity lacunary species,  $\{\text{W}_{16}\}$ . That clearly indicates that the  $\text{V}^{\text{IV}}$  metal center occupies a cap position. On the contrary, the  $\text{V}^{\text{IV}}$  metal center in the Mo-based system is disordered over 18 positions and does not present any preference for a specific site (cap or belt). All of the above observations are in excellent agreement with the EPR studies, which showed the existence of a single  $\text{V}^{\text{IV}}$  site in the case of  $\{\text{V}^{\text{IV}}\text{W}_{17}(\text{V}^{\text{VO}_4})_2\}$  cluster, while in the  $\{\text{V}^{\text{IV}}\text{Mo}_{17}(\text{V}^{\text{VO}_4})_2\}$  capsule, the parameters fit accurately for two distinct, but independent, species.

Moreover, the electrochemical studies in aqueous and organic media showed well separated redox waves for the one electron oxidation of the  $\text{V}^{\text{IV}}$  metal center in the region of 0.500–0.700 V and a typical set of three redox couples in the regions –0.200 to –1.480 V and –0.213 to –0.741 V for the tungsten- and molybdenum-centered reductions, respectively. Additionally, the magnetic behaviors of the two compounds were similar with an  $S = 1/2$  ground state due to the single  $\text{VO}_4^{2+}$  vanadyl constituent in the  $\text{M}_{18}$  shell structure of each cluster, while the temperature-independent  $\chi_{\text{mol}}T$  rules out a scenario in which the 3d electron is localized on one of the  $\text{VO}_4$  templates.

All of these observations mean that these clusters have tremendous potential for the development of new catalysts, electronic materials, and devices. In further work, we will try and expand our studies by site-specific introduction of  $d^1$  transitional metals on the shell (e.g., additional  $\text{V}^{\text{IV}}$ ) of the molecular capsules in order to finely tune their magnetic, electronic, and catalytic properties (preliminary studies show that  $\{\text{V}^{\text{IV}}\text{W}_{17}(\text{V}^{\text{VO}_4})_2\}$  is a more efficient catalyst than  $\{\text{V}^{\text{IV}}\text{Mo}_{17}(\text{V}^{\text{VO}_4})_2\}$  for the oxidation of benzyl alcohol, see Supporting Information).

## ASSOCIATED CONTENT

**Supporting Information.** The CID-MS spectrum details, CV, PXRD, catalytic details, and W-band EPR spectra. This material is available free of charge via the Internet at <http://pubs.acs.org>.

## AUTHOR INFORMATION

### Corresponding Authors

\*Fax: +44 141 330 4888. E-mail: [L.Cronin@chem.gla.ac.uk](mailto:L.Cronin@chem.gla.ac.uk); [harism@chem.gla.ac.uk](mailto:harism@chem.gla.ac.uk). Website: <http://www.chem.gla.ac.uk/staff/lee> or <http://www.croninlab.com>.

## ACKNOWLEDGMENT

We thank the ESPRC, WestCHEM, the University of Glasgow, and the multifrequency EPR Service (Manchester). H.N.M. thanks the Royal Society of Edinburgh and Marie Curie Actions for the financial support. L.C. thanks the Royal Society and Wolfson Foundation for a merit award.

## REFERENCES

- (1) (a) Pope, M. T. In *Heteropoly and Isopoly Oxometalates*; Springer-Verlag: Berlin, 1983. (b) Pope, M. T.; Müller, A. *Angew. Chem., Int. Ed.* **1991**, *30*, 34. (c) *Polyoxometalates: From Platonic Solids to Anti-Retroviral Activity*; Pope, M. T., Müller, A., Eds.; Kluwer Academic Publishers: Dordrecht, Netherlands, 1994. (d) *Polyoxometalate Chemistry From Topology via Self-Assembly to Applications*; Pope, M. T., Müller, A., Eds.; Kluwer Academic Publishers: Dordrecht, Netherlands, 2001. (e) *Polyoxometalate Chemistry for Nano-Composite Design*; Yamase, T., Pope, M. T., Eds.; Kluwer Academic/Plenum Publishers: New York, 2002. (f) *Polyoxometalate Molecular Science*; Borrás-Almenar, J. J., Coronado, E., Müller, A., Pope, M. T., Eds.; Kluwer Academic Publishers: Dordrecht, Netherlands, 2003; NATO Science Series II, Vol. 98. (g) *Comprehensive Coordination Chemistry. II: From Biology to Nanotechnology*; McCleverty, J. A., Meyer, T. J., Eds.; Elsevier: Oxford, 2004.
- (2) (a) Allcock, H. R.; Bissell, E. C.; Shawl, E. T. *J. Am. Chem. Soc.* **1972**, *94*, 8603. (b) Allcock, H. R.; Bissell, E. C.; Shawl, E. T. *Inorg. Chem.* **1973**, *12*, 2963.
- (3) (a) Müller, A.; Beckmann, E.; Bögge, H.; Schmidtman, M.; Dress, A. *Angew. Chem., Int. Ed.* **2002**, *41*, 1162. (b) Müller, A.; Kögerler, P.; Kuhlmann, C. *Chem. Commun.* **1999**, 1347. (c) Gouzerh, P.; Che, M. *Actual. Chim.* **2006**, *298*, 9. (d) Miras, H. N.; Cooper, G. J. T.; Long, D.-L.; Bögge, H.; Müller, A.; Streb, C.; Cronin, L. *Science* **2010**, *327*, 72. (e) Long, D.-L.; Tsunashima, R.; Cronin, L. *Angew. Chem., Int. Ed.* **2010**, *49*, 1736.
- (4) Pope, M. T. *Inorg. Chem.* **1972**, *11*, 1973.
- (5) Sadakane, M.; Steckhan, E. *Chem. Rev.* **1998**, *98*, 219.
- (6) Kozhevnikov, V. *Chem. Rev.* **1998**, *98*, 171.
- (7) Rhule, J. T.; Neiwert, W. A.; Hardcastle, K. I.; Do, B. T.; Hill, C. L. *J. Am. Chem. Soc.* **2001**, *123*, 12101.
- (8) Müller, A.; Luban, M.; Schröder, C.; Modler, R.; Kögerler, P.; Axenovich, M. J.; Schnack, M. J.; Canfield, P.; Budko, S.; Harrison, N. *ChemPhysChem.* **2001**, *2*, 517.
- (9) Müller, A.; Kögerler, P.; Dress, A. W. M. *Coord. Chem. Rev.* **2001**, *222*, 193.
- (10) (a) Way, M.; Bond, A. M.; Wedd, A. G. *Inorg. Chem.* **1997**, *36*, 2826. (b) Thiel, J.; Ritchie, C.; Miras, H. N.; Streb, C.; Mitchell, S. G.; Boyd, T.; Ochoa, M. N. C.; Rosnes, M. H.; McIver, J.; Long, D.-L.; Cronin, L. *Angew. Chem., Int. Ed.* **2010**, *49*, 6984. (c) Yan, J.; Long, D.-L.; Miras, H. N.; Cronin, L. *Inorg. Chem.* **2010**, *49*, 1819.
- (11) (a) Richardt, P. J. S.; White, J. M.; Tregloan, P. A.; Bond, A. M.; Wedd, A. G. *Can. J. Chem.* **2001**, *79*, 613. (b) Peng, Z. H. *Angew. Chem., Int. Ed.* **2004**, *43*, 930. (c) Boyd, T.; Mitchell, S. G.; Miras, H. N.; Long, D.-L.; Cronin, L. *Dalton Trans.* **2010**, *39*, 6460.
- (12) Zeng, H. D.; Newkome, G. R.; Hill, C. L. *Angew. Chem., Int. Ed.* **2000**, *39*, 1772.
- (13) Oglario, F.; de Visser, S. P.; Cohen, S.; Sharma, P. K.; Shaik, S. *J. Am. Chem. Soc.* **2002**, *124*, 2806.
- (14) (a) Long, D.-L.; Abbas, H.; Kögerler, P.; Cronin, L. *Angew. Chem., Int. Ed.* **2005**, *44*, 3415. (b) Mitchell, S. G.; Streb, C.; Miras, H. N.; Boyd, T.; Long, D.-L.; Cronin, L. *Nature Chem.* **2010**, *2*, 308.

(c) Ritchie, C.; Streb, C.; Thiel, J.; Mitchell, S. G.; Miras, H. N.; Long, D.-L.; Boyd, T.; Peacock, R. D.; McGlone, T.; Cronin, L. *Angew. Chem., Int. Ed.* **2008**, *47*, 6881.

(15) Kögerler, P.; Cronin, L. *Angew. Chem., Int. Ed.* **2005**, *44*, 844.

(16) Neumann, R.; Khenkin, A. M. *Chem. Commun.* **2006**, 2529.

(17) (a) Vasylyev, M. V.; Neumann, R. *J. Am. Chem. Soc.* **2004**, *126*, 884. (b) Mbomekalle, I. M.; Keita, B.; Nadjo, L.; Berthet, P.; Hardcastle, K. I.; Hill, C. L.; Anderson, T. M. *Inorg. Chem.* **2003**, *42*, 1163.

(18) Mizuno, N.; Yamaguchi, K.; Kamata, K. *Coord. Chem. Rev.* **2005**, *249*, 1944.

(19) Cronin, L. *Angew. Chem., Int. Ed.* **2006**, *45*, 3576.

(20) (a) Bassil, B. S.; Nellutla, S.; Kortz, U.; Stowe, A. C.; Van Tol, J.; Dalal, N. S.; Keita, B.; Nadjo, L. *Inorg. Chem.* **2005**, *44*, 2659. (b) Stowe, A. C.; Nellutla, S.; Dalal, N. S.; Kortz, U. *Eur. J. Inorg. Chem.* **2004**, 3792. (c) Stamatatos, T. C.; Foguet-Albiol, D.; Wernsdorfer, W.; Abboud, K. A.; Christou, G. *Chem. Commun.* **2011**, *47*, 274. (d) Manoli, M.; Inglis, R.; Manos, M. J.; Nastopoulos, V.; Wernsdorfer, W.; Brechin, E. K.; Tasiopoulos, A. J. *Angew. Chem., Int. Ed.* **2011**, *50*, 4441. (e) Tasiopoulos, A. J.; Vinslava, A.; Wernsdorfer, W.; Abboud, K. A.; Christou, G. *Angew. Chem., Int. Ed.* **2004**, *43*, 2117. (f) Ritchie, C.; Ferguson, A.; Nojiri, H.; Miras, H. N.; Song, Y.-F.; Long, D.-L.; Burkholder, E.; Murrie, M.; Kögerler, P.; Brechin, E. K.; Cronin, L. *Angew. Chem., Int. Ed.* **2008**, *47*, 5609.

(21) (a) Lehmann, J.; Gaita-Ariño, A.; Coronado, E.; Loss, D. *Nature Nanotechnol.* **2007**, *2*, 312. (b) Fleming, C.; Long, D.-L.; McMillan, N.; Johnston, J. B.; Dhanak, N. V.; Gadegaard, N.; Kögerler, P.; Cronin, L.; Kadodwala, M. *Nature Nanotechnol.* **2008**, *3*, 289.

(22) Long, D.-L.; Kögerler, P.; Farrugia, J.; Cronin, L. *Dalton Trans.* **2005**, 1372.

(23) (a) Long, D.-L.; Kögerler, P.; Cronin, L. *Angew. Chem., Int. Ed.* **2004**, *43*, 1817. (b) Miras, H. N.; Ochoa, M. N. C.; Long, D.-L.; Cronin, L. *Chem. Commun.* **2010**, 8148.

(24) Miras, H. N.; Long, D.-L.; Kögerler, P.; Cronin, L. *Dalton Trans.* **2008**, 214.

(25) (a) Miras, H. N.; Yan, J.; Long, D.-L.; Cronin, L. *Angew. Chem., Int. Ed.* **2008**, *47*, 8420. (b) Wilson, E. F.; Abbas, H.; Duncombe, B. J.; Streb, C.; Long, D.-L.; Cronin, L. *J. Am. Chem. Soc.* **2008**, *130*, 13876. (c) Pradeep, C. P.; Long, D.-L.; Newton, G. N.; Song, Y.-F.; Cronin, L. *Angew. Chem., Int. Ed.* **2008**, *23*, 4388. (d) Miras, H. N.; Stone, D. J.; McInnes, E. J. L.; Raptis, R. G.; Baran, P.; Chilas, G. I.; Sigalas, M. P.; Kabanos, T. A.; Cronin, L. *Chem. Commun.* **2008**, 4703. (e) Miras, H. N.; Wilson, E. F.; Cronin, L. *Chem. Commun.* **2009**, 1297. (f) Miras, H. N.; Wilson, E. F.; Rosnes, M. H.; Cronin, L. *Angew. Chem., Int. Ed.* **2011**, *50*, 3720.

(26) Long, D.-L.; Kögerler, P.; Farrugia, J.; Cronin, L. *Angew. Chem., Int. Ed.* **2003**, *42*, 4180.

(27) (a) Deery, M. J.; Howarth, O. W.; Jennings, K. R. *J. Chem. Soc., Dalton Trans.* **1997**, *24*, 4783. (b) Waters, T.; O'Hair, R. A. J.; Wedd, A. G. *J. Am. Chem. Soc.* **2003**, *125*, 3384. (d) Ohlin, C. A.; Villa, E. M.; Fettinger, J. C.; Casey, W. H. *Angew. Chem., Int. Ed.* **2008**, *47*, 8251.

(28) (a) Cao, X.; Naruke, H.; Yamase, T. *Acta Crystallogr.* **2003**, *E59*, 318. (b) Fuchs, J.; Palm, R. Z. *Naturforsch., B: Chem. Sci.* **1984**, *39*, 757. (c) Massart, R.; Contant, R.; Fruchart, J. M.; Ciabrini, J. P.; Fournier, M. *Inorg. Chem.* **1977**, *16*, 2916. (d) Robert, F.; Teze, A. *Acta Crystallogr.* **1981**, *B37*, 318.